Phys. Med. Biol. **42** (1997) 177–198. Printed in the UK PII: S0031-9155(97)70817-0

Characterization of *post mortem* arterial tissue using time-resolved photoacoustic spectroscopy at 436, 461 and 532 nm

P C Beard and T N Mills

Department of Medical Physics and Bioengineering, University College London, Shropshire House, 11–20 Capper Street, London WC1E 6JA, UK

Received 1 January 1996, in final form 13 September 1996

Abstract. Time-resolved photoacoustic spectroscopy has been used to characterize *post mortem* arterial tissue for the purpose of discriminating between normal and atheromatous areas of tissue. Ultrasonic thermoelastic waves were generated in *post mortem* human aorta by the absorption of nanosecond laser pulses at 436, 461 and 532 nm produced by a frequency doubled Q-switched Nd:YAG laser in conjunction with a gas filled Raman cell. A PVDF membrane hydrophone was used to detect the thermoelastic waves. At 436 nm, differences in the photoacoustic signatures of normal tissue and atherorma were found to be highly variable. At 461 nm, there was a clear and reproducible difference between the photacoustic response of atheroma and normal tissue as a result of increased optical attenuation in atheroma. At 532 nm, the generation of subsurface thermoelastic waves provided a means of determining the structure and thickness of the tissue sample. It is suggested that pulsed photoacoustic spectroscopy at 461 and 532 nm may find application in characterizing arterial tissue *in situ* by providing information about both the composition and thickness of the vessel wall.

1. Introduction

It is of interest to characterize arterial tissue for two reasons. Firstly, in the treatment of narrowed blood vessels using minimally invasive techniques such as laser angioplasty, balloon angioplasty or atherectomy, which remove or displace occlusive material, it is necessary to acquire information about the composition and thickness of the vessel wall. This is to ensure that only diseased areas are treated and damage to the normal vessel wall is minimized. Secondly, it would be useful to have a technique for characterizing arterial tissue which could be used to provide information on the evolution of atherosclerosis. Such a technique would enable the progress of the disease to be monitored by performing periodic intraluminal investigations in order to decide the point at which treatment is necessary.

Various techniques for the *in situ* characterization of vascular tissue have been investigated although the twin requirements of being able to measure the composition and thickness of the vessel wall have yet to be fulfilled. In fluorescence spectroscopy, the tissue is excited to fluoresce using low-power laser light (Deckelbaum *et al* 1987, Andersson-Engels *et al* 1990, Oraevsky *et al* 1993). It has been shown that the broad fluoresence spectra of atheromatous plaques is different to that of normal vascular tissue although the large background fluorescence can make it difficult to pick out individual spectral features. Raman spectroscopy of calcified (Clarke *et al* 1987) and soft fatty plaques (Clarke *et al* 1988) in vascular tissue was initially performed using 514 nm laser excitation and revealed

0031-9155/97/010177+22$19.50

the presence of a number of shifts which were not observed in normal tissue. Near infrared Fourier transform Raman spectroscospy (Baraga *et al* 1992) has shown that a wide range of vascular components can be identified and it has been suggested that this technique may have a role as a means of performing *in situ* histochemical examinations. Pulsed photothermal radiometry of arterial tissue at 488 nm has also been investigated (Long and Deutsch 1987) and was shown to be capable of discriminating between normal tissue and atheromatous plaque at this wavelength. The optical techniques described above lend themselves to intraluminal use since the light to and from the tissue can in some cases be delivered via an optical fibre inserted into the blood vessel. The disadvantage is that they are unable to provide spatial information regarding the structure of the vessel. Ultrasound can provide spatial information using a transducer operating in pulse-echo mode and can be implemented *in situ* using intravascular ultrasound (IVUS) probes. Tissue characterization can also be performed to a degree using ultrasound (Gussenhoven *et al* 1989, Chong *et al* 1993) although with far less detail of individual vascular components than can be provided by the optical techniques.

A technique that has the potential to provide both composition and thickness information is that of time resolved photoacoustic spectroscopy. In this technique, sub-ablation threshold nanosecond laser pulses are absorbed in the tissue, producing ultrasonic thermoelastic waves. The amplitude and temporal characteristics of the thermoelastic waves depend strongly upon the optical properties of the tissue and it has been suggested that, by exploiting the preferential optical attenuation in atheroma in the spectral range 420–530 nm (Prince *et al* 1986), the photoacoustic signature could be used to identify atheromatous plaque (Mills 1988, Mills *et al* 199l). In addition, the reflection and generation of subsurface thermoelastic waves can provide information about the structure and thickness of the vessel wall. It is therefore a dual sensing technique combining the spectroscopic nature of the optical techniques discussed above with the thickness measuring abilities of ultrasound. *In vitro* time resolved photoacoustic measurements of the type discussed in this paper have been reported by others. Al Dhahir *et al* (1990) measured optical attenuation via the photoacoustic signature using a pulsed dye laser and confirmed the preferential attenuation in atheroma over the range 440–500 nm. Crazzolara *et al* (1991) also showed that the photoacoustic signature of calcified plaques, using an excimer laser at 308 nm, is different to that of normal arterial tissue. Such measurements provide preliminary experimental evidence that this type of photoacoustic spectroscopy could be used to characterize arterial tissue. For its practical *in vivo* implementation, various schemes have also been described. These include a miniature all-optical intravascular photoacoustic probe (Mills 1988, Beard and Mills 1995) using a transparent Fabry–Perot ultrasound sensor (Beard and Mills 1996) at the end of an optical fibre to detect the thermoelastic waves. A hybrid scheme using a piezoelectric transducer for detection has also been described (Chen *et al* 1993).

The aim of the work described in this paper was to exploit the increased optical absorption in atheroma, reported by others, between 420 and 530 nm for discrimination purposes. For this reason, laser pulses at 436 and 461 nm were used to generate photacoustic signatures in arterial tissue. This approach is somewhat non-specific as it signifies the presence of atheroma but provides little further information about the tissue. An additional aim of the work, therefore, was to obtain thickness information using 532 nm laser pulses. At this wavelength the light penetrates the full thickness of the tissue, producing a corresponding photoacoustic contribution that extends from the surface of the tissue (intima) to the lowermost layer (adventitia). A significant part of the work described in this paper is the use of a non-scattering liquid absorber of known and adjustable optical properties as a target absorber. This enabled us to characterize the experimental technique used and study

the dependence of the photoacoustic signature on optical absorption.

Since the photoacoustic response of arterial tissue is dependent upon the optical and acoustic properties of the tissue, these are discussed in section 2. This is followed in section 3 by consideration of the mechanism by which thermoelastic waves are generated by the absorption of nanosecond laser pulses. Section 4 describes the experimental method and results obtained in a non-scattering liquid absorber and *post mortem* human aorta.

2. Optical and acoustic properties of arterial tissue

2.1. Optical properties

The optical properties of arterial tissues have been measured *in vitro* by a number of workers. Van Gemert *et al* (1985) obtained the Kubelka–Munk absorption and scattering coefficients in normal and atheromatous plaque at three commonly available laser wavelengths: 514.5, and 633 nm and 1.06 μm. It was noted that only at 514.5 nm was there higher absorption in the plaque specimen. The first comprehensive measurements of the optical properties of normal and atheromatous aortic tissue, also in terms of the Kubelka–Munk coefficients, were made by Prince *et al* (1986) over the wavelength range 250 nm–1.25 μm. It was noted that in soft yellow fibro-fatty plaques there was preferential absorption in the spectral range 420–530 nm, peaking at about 470 nm when absorption was at least twice that in normal areas of tissue. Carotenoids within the plaque mass were identified as the chromophore responsible for the increased absorption in the atheroma. Others have also reported preferential attenuation in atheroma around 470 nm, using a variety of techniques, although the effect has not always been specifically attributed to preferential absorption (Oraevsky *et al* 1988, Al Dhahir *et al* 1990, Long and Deutsch 1987). In general, scattering in soft tissues varies little with wavelength so it is likely that any preferential attenuation observed is in fact due to increased absorption. Although the most comprehensive data on both normal and atheromatous arterial tissue are those obtained by Prince *et al* (1986) they have the disadvantage that the data were analysed using Kubelka-Munk theory. This theory is no longer considered to provide an accurate description of light propagation in biological tissues, particularly in terms of providing absolute values of optical coefficients. Despite this limitation, two conclusions can still be drawn from the work of Prince *et al* (1986): firstly, that there is an increase in optical attenuation in arterial tissue in the spectral range 420–530 nm, and, secondly, that this is due to increased absorption rather than scattering.

In terms of the absolute optical absorption and scattering coefficients of arterial tissue the work of Keijzer *et al* (1989b) is more useful. Integrating sphere measurements of the intima, media and adventitia of normal aortic samples were made separately and the transport coefficients (as opposed to Kubelka–Munk coefficients) were obtained using diffusion theory. Optical coefficients at the three wavelengths of interest in this study are shown in table 1 where μ_a and μ_s are the absorption and scattering coefficients respectively and g is the mean cosine of scattering angle. The data in table 1 show that there are significant differences in the values of μ_a for the different tissue layers. It also shows, in common with most soft tissues, that scattering dominates. Since the study did not include atheromatous samples, the presence of preferential absorption observed by Prince *et al* (1986) was not confirmed.

A difficulty with measurements of the optical properties of layered biological media, such as arterial tissue, is that they are often found to differ widely, making comparisons between different workers difficult. This is due to the use of different measurement techniques and theoretical analyses and the heterogeneous nature of the tissue. Atheroma

Table 1. Optical coefficients of normal arterial tissue (Keijzer *et al* 1989b).

λ (nm)	Tissue layer	μ_a (cm^{-1})	μ_s (cm^{-1})	g
	intima	36	320	0.85
436	media	12	505	0.91
	adventitia	42	330	0.78
	intima	16	300	0.85
461	media	8	490	0.91
	adventitia	21	305	0.78
	intima	10	220	0.85
532	media	5	400	0.90
	adventitia	12	270	0.91

is particularly complex as the composition of a raised fibrous–fatty plaque of a particular thickness can vary between the extremes of either predominantly all-lipid or all-fibrous material. Additional complicating factors include calcification, the presence of intramural thrombi and vascularization. These factors are of particular significance when attempting to exploit preferential absorption in atheroma for discrimination purposes as the presence of preferentially absorbing chromophores within the plaque mass can vary greatly.

2.2. Acoustic properties

The acoustic properties of non-calcified arterial tissue, with the exception of attenuation, are similar to those of water (Goss *et al* 1978). The velocity of sound in aortic tissue has been measured *in vitro* with values ranging from 1492 to 1650 m s^{-1} (Greenleaf *et al* 1974, Rooney *et al* 1982). The variation was mainly attributed to differences in collagen content. As is to be expected, calcified lesions have significantly higher velocities, in the range 1900–2000 m s^{-1}. The acoustic impedance of normal artery wall and fibrous-fatty plaques has been measured as being in the range $1.53–1.86 \times 10^6$ kg m^{-2} s^{-1} (Greenleaf *et al* 1974). Acoustic impedance differences at the boundaries of the different layers in uncalcified tissue are of the order of only a few per cent. Attenuation in non-calcified tissue shows more variation than the other acoustic properties with values of around 6 dB cm^{-1} at 10 MHz for the normal artery wall and 5.6–28.9 dB cm^{-1} for fibrous–fatty lesions at the same frequency (Greenleaf *et al* 1974). Apart from attenuation, the differences in acoustic properties between normal and atheromatous tissue are small compared to the differences in optical properties.

3. Photoacoustic generation in arterial tissue

The important features of photoacoustic generation are discussed qualitatively in the first instance using a simple theory based on thermal expansion in an optically non-scattering liquid. This theory is then modified to take into account the effects of scattering that are present in tissues. Consideration is given to using the photoacoustic signature to discriminate between atheroma and normal tissue and obtain information relating to the thickness of the tissue.

3.1. Thermoelastic wave generation in a non-scattering absorber

Consider a pulsed laser beam incident on a homogeneous, non-scattering liquid absorber as shown in figure 1. The irradiance decreases exponentially along the axis of the laser beam in accordance with Lambert's law

$$I(z) = I(0)\,\mathrm{e}^{-\mu_a z} \tag{1}$$

where $I(z)$ is the irradiance at depth z, $I(0)$ is the irradiance at the surface of the absorber and μ_a is the optical absorption coefficient. The energy of the optical pulse is absorbed producing a thermal gradient in the liquid. Rapid thermal expansion occurs leading to acoustic energy propagating away from the source. For efficient acoustic generation, the duration of the optical pulse should be sufficiently short so that both thermal and stress confinement takes place. To fulfil the condition of thermal confinement, the optical pulse duration should be short compared to the thermal relaxation time of the heated volume so that there is no significant heat loss by thermal diffusion during the heating process. For stress confinement, the optical pulse duration should be sufficiently short that the process of heat deposition is faster than that of thermal expansion. This requires a pulse duration that is short compared to the stress relaxation time—the time taken for the thermoelastic wave to propagate a distance equal to the optical penetration depth. The geometry of the acoustic source approximates to that of a cylinder of radius R and length $1/\mu_a$ where R is the radius of the incident laser beam and $1/\mu_a$ is the optical penetration depth. When R is large compared to the penetration depth (the one dimensional case), we need consider only the acoustic waves propagating above and below the source. Using a simplified model of one-dimensional thermal expansion in a liquid (Patel and Tam 1981, Mason and Thurston 1988), the pressure $P(z)$ at each point along the absorbing volume can be expressed as

$$P(z) = \beta B E \mu_a\,\mathrm{e}^{-\mu_a z}/\rho C_p \pi R^2 \tag{2}$$

where B is the bulk modulus of the liquid, β is the coefficient of volume thermal expansion, ρ is the density, C_p is the specific heat and E is the energy of the optical pulse. Inspection of equation (2) shows that the amplitude of the thermoelastic wave is proportional to the optical absorption coefficient. Equation (2) also shows that there is an exponentially decreasing spatial distribution of pressure sources in the absorbing volume. Although this equation does not provide a complete description of the temporal characteristics of the thermoelastic wave (solution of the one-dimensional wave equation is required for this (Carome *et al* 1964, Gournay 1966, Sigrist 1986)), it does suggest that at some point in the time history of the wave there will be an exponential component that is dependent upon the absorption coefficient. In particular, when measuring from above the source it can be expected that the acoustic pressure will fall exponentially in time (with exponential constant $\mu_a c$, where c is the velocity of sound in the liquid) from a maximum corresponding to the pressure contribution from $z = 0$. Conversley, when detecting the thermoelastic wave propagating below the source, the acoustic pressure will increase exponentially (with exponential constant $\mu_a c$) to a maximum that corresponds to the contribution from $z = 0$. By fitting an exponential to the appropriate part of the thermoelastic wave (above or below source) and with knowledge of the speed of sound, a value of μ_a can therefore be obtained. A useful advantage of analysing the temporal characteristics (as opposed to amplitude characteristics) of the thermoelastic wave is that the value of μ_a is independent of variations in incident laser pulse energy, detector sensitivity and source–detector alignment.

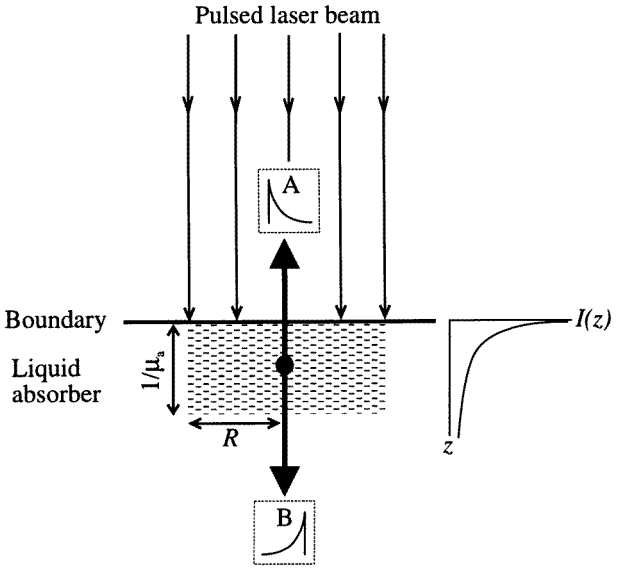

Figure 1. Generation of thermoelastic waves propagating above (A) and below source (B) due to absorption of short laser pulses in a non-scattering liquid absorber.

3.2. Thermoelastic wave generation in a scattering absorber

For a target in which scattering dominates, as is the case with arterial tissue (Keijzer *et al* 1989b), the axial light distribution in a semi-infinite slab of homogenous tissue illuminated by a large-area collimated beam can be modelled using diffusion theory (Star *et al* 1988). At a certain depth beneath the tissue surface, the light becomes diffuse and the irradiance decreases exponentially with exponential constant μ_{eff} such that

$$I(z) = I(0)k\,\mathrm{e}^{-\mu_{eff}z} \tag{3}$$

where k is a constant. μ_{eff} is the effective attenuation coefficient; it is a function of μ_a and μ_s and is given by

$$\mu_{eff} = \sqrt{3\mu_a[\mu_a + (1-g)\mu_s]} \tag{4}$$

where g is the mean cosine of the scattering angle. Since the axial light distribution is exponential, the expression for the acoustic pressure at each point in the absorbing volume below the depth at which the light becomes diffuse is of a form similar to equation (2) with μ_a replaced by μ_{eff}. The amplitude of the thermoelastic wave is therefore proportional to μ_{eff} We can also, using the same arguments as in 3.1, expect an exponentially decreasing component (when measuring from above the target) in the part of the thermoelastic wave that corresponds to tissue depths beyond which the light has become diffuse. The exponential constant will be $\mu_{eff}c$ and so, by fitting an exponential to this part of the wave, a value for μ_{eff} can be obtained. It has been suggested that the depth beyond which the light can be considered to be diffuse in predominantly scattering media is somewhere between one and ten transport mean free paths (Wang and Jacques 1992, Keijser *et al* 1989a, Star *et al* 1988). The transport mean free path is given by $1/(\mu_a + (1-g)\mu_s)$ and using the data in table 1 gives a typical value of approximately 200 μm for arterial tissue. In the region where the light is not diffuse, close to the tissue surface, the light distribution can

be complex and may exceed the surface irradiance due to backscattering. Such behaviour will also manifest itself in a complex manner in the temporal characteristics of the initial part of the thermoelastic wave.

3.3. Detection of atheroma

As described in subsection 3.2, the amplitude and temporal characteristics of the thermoelastic wave depend upon the effective attenuation coefficient μ_{eff} of the tissue which in turn is a function of the absorption coefficient μ_a. Since the ratio of optical absorption in atheroma to normal tissue at 470 nm (Prince *et al* 1986) is approximately a factor of two, there will be significant differences between the photoacoustic signatures of the two tissue types, thus providing a means of discriminating between normal and atheromatous tissue. Although subsection 2.2 indicated that there are differences in the acoustic properties of non-calcified arterial tissue, these are very small compared to the differences in optical properties of the tissue and are not expected to contribute significantly to differences in the photoacoustic signature. Calcified plaques are not specifically considered in this paper although they should be straightforward to detect as both optical and acoustic characteristics are very different from normal tissue, producing a highly individual photoacoustic signature.

3.4. Thickness measurement

Measurements of the thickness of the tissue can be made in two ways. The first is by measuring the time of arrival of acoustic reflections from subsurface layers at which an acoustic impedance mismatch occurs. Since acoustic impedance mismatches between the layers of non-calcified arterial tissue are very small, high detection sensitivities and high optical pulse energies (possibly close to the damage threshold of the tissue) would be required to achieve this. An alternative method of acquiring spatial information is to choose an optical wavelength such as 532 nm that penetrates the full thickness of the tissue. This enables subsurface thermoelastic waves to be generated at the boundaries of tissue layers where there is a change in optical properties. Measurement of the time of arrival of these waves allows the thickness of the layers to be measured. Evidence of the feasibility of this concept is provided by the measurements of Keijzer *et al* (1989b) (table 1), which showed that the optical properties of the intima, media and adventitia of normal aortic tissue are signficantly different.

3.5. Pulse energy considerations

The fluence incident on the tissue must be below the threshold at which irreversible changes occur yet sufficient to produce thermoelastic waves that can be readily detected. The ablation threshold of normal arterial tissue for a 10 ns pulse at 532 nm is in excess of 10 mJ mm^{-2} (Boulnois 1986, Cross *et al* 1987). Irreversible changes in tissue may occur at fluences somewhat below the ablation threshold and consideration should also be given to the possibility of damage to tissue by the mechanical disruption of tissue layers as a result of the generation and propagation of the thermoelastic wave. For these reasons it would be sensible to limit the incident fluence to around 1 mJ mm^{-2}.

4. Experimental details

An experimental arrangement was set up to generate and detect thermoelastic waves in different media. Measurements were carried out initially at 532 nm using a non-scattering liquid absorber of known optical properties. These measurements enabled the experimental method to be characterized and the photoacoustic process to be studied as a function of optical absorption μ_a. The liquid absorber used was a readily available writing ink ('washable' blue Solv-X Quink ink), which was diluted with an acidic buffer (Tris, pH 3) to obtain a range of stable solutions of different values of μ_a. Optical transmission measurements at 532 nm were used to confirm that these solutions were non-scattering and obeyed the Beer–Lambert law.

To study the photoacoustic signals generated in arterial tissue, measurements on 15 *post mortem* human aortas at three wavelengths, 436, 461 and 532 nm, were made. Each specimen was kept refrigerated at 4 °C and used within 6 h of excision. Areas of atheroma were identified by macroscopic inspection and only soft yellow, predominantly lipid plaques were selected as atheromatous samples. In each case, the fat layer adjacent to the adventitia was removed and the aorta specimens stored in saline until use.

4.1. Experimental arrangement and procedure

The experimental set-up shown in figure 2 was used for both the ink and tissue experiments. Figure 2 shows the experimental arrangement with a tissue sample in place.

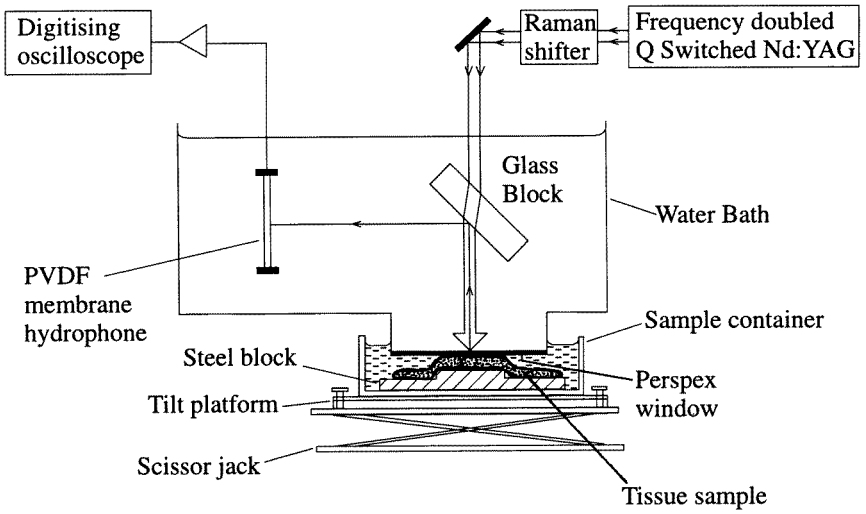

Figure 2. The experimental arrangement for the generation and detection of thermoelastic waves.

4.1.1. The laser system. Laser pulses at 436, 461 and 532 nm were obtained using a laser system that consisted of a Q switched, frequency doubled, Nd:YAG laser and a gas filled Raman cell. 532 nm optical pulses of nanosecond duration were obtained using the direct output of the frequency doubled Nd:YAG laser. The diameter of the beam was 3 mm. To obtain optical pulses at 436 and 461 nm, the Raman cell was used to shift the 532 nm

output of the Nd:YAG. When the Raman cell was filled with hydrogen it provided shifts in wavenumber of 4155 cm^{-1} enabling an output at 436 nm to be obtained by selecting the first anti-Stokes shift. Similarly, when the Raman cell was filled with methane, the wavenumber shift of 2914 cm^{-1} enabled 461 nm to be obtained also by selection of the first anti-Stokes shift.

4.1.2. Ink experiments. Experiments were carried out at 532 nm to examine the characteristics of the thermoelastic waves propagating above and below the source that were generated in different ink–Tris concentrations. The sample container was filled with ink of the required concentration. The container was placed on a tilt platform attached to a modified scissor jack and raised until the ink was in contact with the Perspex window. The output beam from the laser system was directed on to the ink absorber producing a thermoelastic wave that propagated vertically upwards (i.e. above source) through the Perspex window. A second thermoelastic wave was also generated simultaneously that propagated vertically downwards (i.e. below source) through approximately a 5 mm thickness of ink and was subsequently reflected from the steel block at the bottom of the container to follow precisely the same path as the upwards travelling wave. The thermoelastic waves arrived at a PVDF membrane hydrophone after reflection from a glass block angled at 45° acting as an acoustic reflector. The total acoustic path length from source to hydrophone was approximately 6 cm and was essentially the same for both above- and below-source thermoelastic waves. The hydrophone was a calibrated 25 MHz 50 μm bilaminar PVDF membrane hydrophone (Marconi Y-33-7611) of active diameter 1 mm and sensitivity 100 mV MPa^{-1}. This type of hydrophone is widely acknowledged as the gold standard in ultrasound measurement on account of its wideband uniform frequency response, linearity, stability and minimum perturbation to the acoustic field under measurement. The flat frequency response of the hydrophone in particular is an essential requirement for analysing the temporal characteristics of thermoelastic waves. The output of the hydrophone was displayed and averaged over 30 shots using a 500 MHz digitizing oscilloscope.

Alignment of the hydrophone with the incident thermoelastic waves was carried out optically with the sample container empty. The low-power frequency doubled fixed-Q output of the Nd:YAG laser was used as an alignment beam to mimic the path of the thermoelastic waves. The position of the hydrophone was adjusted until the Fresnel reflection from the Perspex window was visible on its active area. This ensured that the initial upwards travelling wave was correctly aligned. To ensure that the downwards travelling wave, after reflection from the steel block, was coincident with the upwards travelling thermoelastic wave, a plane parallel mirror was placed on the top surface of the block. The tilt platform was then adjusted so that the reflection from the mirror of the 532 nm Nd:YAG output was visible on the active region of the hydrophone.

4.1.3. Tissue experiments. For these experiments, the experimental set-up shown in figure 2 and the alignment procedures described above were used. The aorta specimen under investigation was immersed in saline in the sample container. The scissor jack was then raised until the top surface of the tissue was in light contact with the Perspex window. To verify that the sensitivity of the experimental set-up remained constant, ink was used as a reference target absorber in place of the tissue sample before and after each set of tissue measurements was taken.

4.2. Results

In the following subsections, the photoacoustic waveforms generated in the ink absorber and *post mortem* human aorta are discussed. The vertical scale of these waveforms represents the acoustic pressure at the surface of the target. This was obtained by applying a correction to take into account the acoustic losses arising from the propagation of the thermoelastic waves through the water, the Perspex window and the reflection from the glass block. For the frequency dependent acoustic losses, such as that due to propagation through water, a frequency of 10 MHz was chosen to calculate the attenuation as this was measured to be approximately the centre frequency of thermoelastic waves generated in tissue. The correction was checked experimentally and found to give a good estimate of the acoustic losses in the experimental arrangement.

4.2.1. Ink experiments. Thermoelastic waves for three different ink–Tris concentrations are shown in figure 3 for measurements above and below the source. When measuring above the source (figure 3(a)), the characteristic shape of the wave is that of an initial compression followed by an absorption dependent exponentially decaying rarefaction. By fitting an exponential to the rarefaction part of the waveform and using a value of 1500 m s^{-1} for the speed of sound, a value for μ_a can be obtained as described in subsection 3.1. When measuring below the source (figure 3(b)) it is the initial, exponentially increasing compression part of the wave that is dependent upon absorption and it is to this part of the wave that an exponential was fitted to in order to obtain μ_a. For both sets of measurements, values of μ_a for nine different ink–Tris concentrations were determined and are shown in figure 4. Figure 4 also shows the straight line representing the known value of μ_a of the ink–Tris solutions as a function of concentration. Both sets of measurements show a linear relation to concentration, as expected. The values of μ_a calculated from the downwards travelling (i.e. below-source) thermoelastic waves are in close agreement with the known values of μ_a. The values of μ_a calculated from the upwards travelling (i.e. above-source) waves however are a factor of 2.8 lower than the known values. It would appear that the rate of exponential decay of the above-source thermoelastic wave is somehow reduced. The amplitudes of both above- and below-source measurements are shown in figure 5 and show a linearly increasing dependence on concentration, as expected.

Note the bipolar shape of the waves measured above the source (figure 3(a)). These are in contrast to the monopolar waveforms predicted by theories that make use of solutions of the 1D wave equation (Carome *et al* 1964, Gournay 1966, Sigrist 1986) for the boundary conditions that exist in the experimental set-up used. This is because detection by the hydrophone in these experiments takes place mainly in the acoustic far field where the thermoelastic wave no longer propagates as a plane wave. It has been shown theoretically and experimentally (Terzic and Sigrist 1984) that, for this source–detector geometry and boundary conditions, the thermoelastic wave generated at source is a monopolar wave and gradually evolves into a bipolar wave as it propagates into the acoustic far field. The far-field signal is in fact the time derivative of the near-field thermoelastic wave (Bozkhov *et al* 1981, Sigrist 1986). In the near field, when measuring above the source, the thermoelastic wave is a compressive monopolar wave consisting of a rapidly increasing positive edge followed by an exponential decrease. The time derivative of this is a positive delta function followed by an exponentially decaying negative component. The delta function is filtered by the finite bandwidth of the hydrophone to give an initial short compressional pulse which is then followed by an exponentially decaying rarefaction as seen in the waveforms shown in figure 3(a). Thus the effect of diffraction is to convert the exponentially decaying

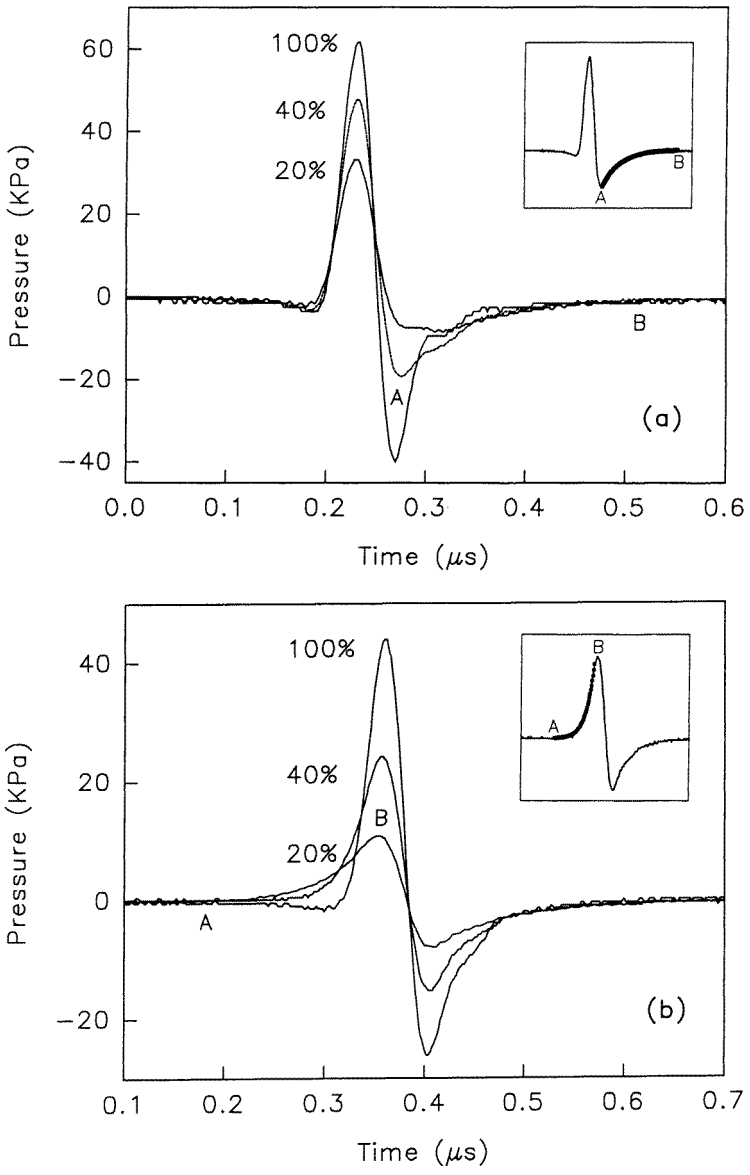

Figure 3. Thermoelastic waves generated (a) above and (b) below the source in three different ink–Tris concentrations. Inset diagrams show the part of the waveform (between A and B) to which an exponential is fitted in order to obtain μ_a. Incident fluence, 0.085 mJ mm^{-2}; pulse duration, 14 ns, acoustic path length, 6 cm.

compressional part of the near-field waveform into an exponentially decaying rarefaction in the far field. Hence the exponential was fitted to the trailing edge of the rarefaction part of the thermoelastic wave when measuring above the source as shown in figure 3(a). When measuring below the source, the situation is effectively reversed so the far-field

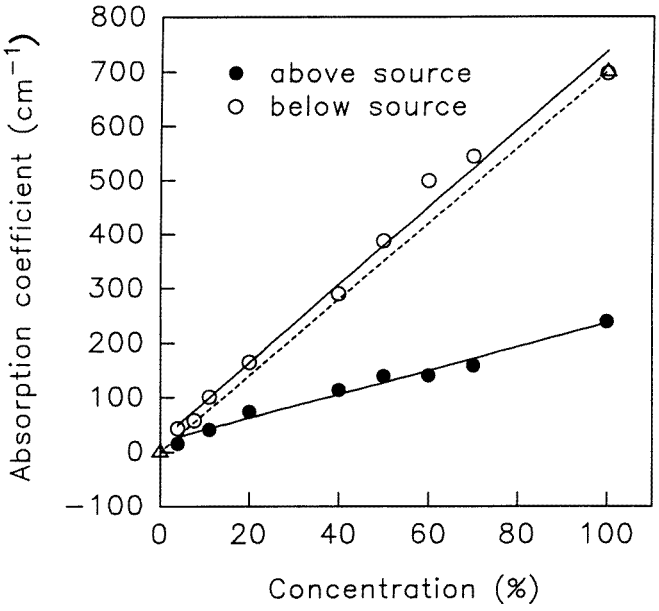

Figure 4. Values of absorption coefficient μ_a calculated by fitting an exponential to thermoelastic waves generated above and below the source in different ink–Tris concentrations. The dashed line represents the known value of μ_a as a function of ink concentration.

thermoelastic wave consists of an exponentially rising compressional component followed by a short rarefaction component (approximating to a negative delta function) as shown in figure 3(b).

The reason for the discrepancy between the above- and below-source values of μ_a shown in figure 4 is unclear. It is unlikely to be due to some difference in the experimental set-up for the two cases as this was the same for the two types of measurement. In particular, the acoustic path length ($\sim$6 cm) travelled by each wave was very nearly the same. The discrepancy may be due to a combination of diffraction effects and the spatial integration of the acoustic field by the hydrophone due its relatively large active area as discussed by Paltauf *et al* (1996). These effects influence the later parts of the thermoelastic wave thus modifying the decaying rarefaction component of the above-source thermoelastic wave which carries the information relating to μ_a. For the below-source wave, although the diffraction effects still influence the later part of the wave, the inital part of the wave, to which the exponential fit is applied to obtain μ_a, is not modified. Hence the below-source values of μ_a agree with the known values. In any practical *in vivo* implementation of the technique, it is likely that measurements will be made on the same side of the target (i.e. above the source). If absolute values of μ_{eff} are required, it would therefore be necessary to take into consideration the effects described above by calibrating the system using a phantom target of variable optical properties and applying an appropriate correction. Ideally, a scheme in which a small-active-area detector can be placed in front of and immediately adjacent to the thermoelastic source should be used so that diffraction effects can be neglected.

The characteristic acoustic wavelength λ_a of the thermoelastic wave should be small compared to the thickness of the hydrophone (in this case 50 μm) for an accurate representation of the whole of the thermoelastic wave. For a non-scattering absorber,

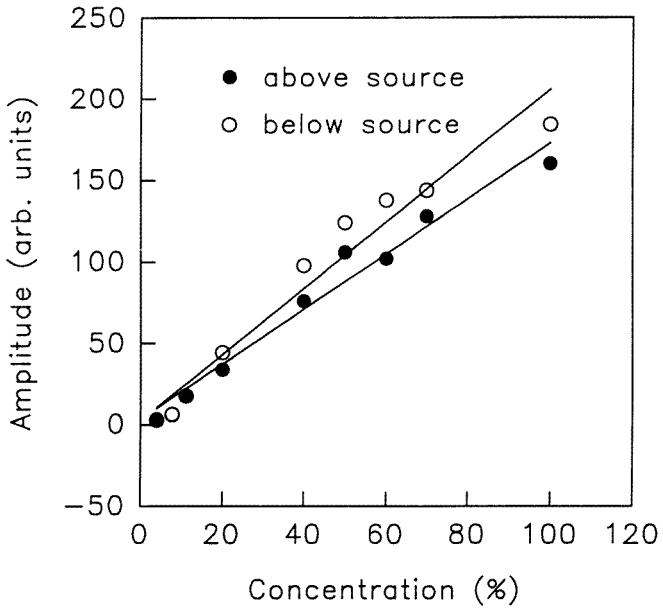

Figure 5. Amplitudes of thermoelastic waves generated above and below source in different ink–Tris concentrations.

$\lambda_a \equiv 2\ \mu_a^{-1}$ (Sigrist 1986). For the highest concentration used in these experiments, $\mu_a = 700\ \text{cm}^{-1}$, and hence $\lambda_a \sim 30\ \mu$m. It might therefore be expected that the shape of the thermoelastic wave would be altered, possibly compromising the values of μ_a obtained at high absorber concentrations. For the specific purpose of obtaining a value of μ_a from the below-source thermoelastic wave, only the initial exponentially increasing part of the wave is used, and for high μ_a it can be shown that the time constant of this part of the thermoelastic wave is not significantly modified by the hydrophone, enabling an accurate value of μ_a to be obtained. The reason for this is that when the hydrophone is acoustically thick (i.e comparable to or thicker than λ_a), the output is proportional to the stress integrated across the depth that the acoustic wave has penetrated into the hydrophone. In the case of an exponentially increasing acoustic wave propagating into the hydrophone (i.e. the initial part of the below-source wave), the output, for high μ_a, is proportional to an expression in which an exponential of the same time constant of the acoustic signal dominates. The same applies to an exponentially decreasing acoustic wave (as is the above-source wave) propagating out of the hydrophone. Thus, values of μ_a that correspond to an acoustic wavelength comparable to or smaller than the thickness of the hydrophone can still be measured. Hence, the data at high μ_a do not deviate significantly from the straight-line fits shown in figure 4. Whilst the hydrophone can, when acoustically thick, give an accurate representation of exponentially varying parts of an acoustic wave that occur at the beginning or end of the wave, this does not apply to other parts of the wave and the overall shape may appear quite different from its true shape. One effect will be to broaden the acoustic wave by a factor related to the acoustic transit time of the wave across the thickness of the hydrophone. Clearly, this will limit the spatial resolution that can be obtained if time-of-arrival type measurements are being made to obtain information about the structure of a target.

4.2.2. Tissue experiments. The photoacoustic signatures generated in normal and atheromatous *post mortem* aorta at 436, 461 and 532 nm are discussed in the following paragraphs. The effective attenuation coefficients were obtained by fitting an exponential decay to the part of the waveform that corresponds to a depth at which the light could be assumed to have become diffuse. In these experiments this depth was assumed to be at least 400 μm—approximately two transport mean free paths. Only the thermoelastic waves generated above the source were studied as it is these waves that would be detected in any practical *in vivo* system. The correction factor discussed in subsubsection 4.2.1 was therefore used to obtain the correct value of μ_{eff}. The speed of sound used throughout was1570 m s^{-1}. Although a large number of measurements of μ_{eff} were made, it was considered that, due to the large variation in the morphology of the different specimens, a statistical analysis would be inappropriate. Selected waveforms of the photoacoustic signals generated at a number of positions on a single aorta specimen are therefore shown at each wavelength. These were chosen to be as representative as possible of the different specimens with variations from these discussed in detail.

λ = *436 nm.* Waveforms generated at four positions on a sample of normal aortic tissue are shown in figure 6(a). The decaying rarefaction part of the waves (between A and B) corresponds spatially to the photoacoustic contribution from the media. By fitting an exponential to this part of the wave a value of $\mu_{eff} = 123$ cm^{-1} was obtained. This is somewhat higher than the value of $\mu_{eff} = 45$ cm^{-1} obtained by inserting the values $\mu_a = 12$ cm^{-1}, $\mu_s = 505$ cm^{-1}, $g = 0.91$ for the media from table 1 (Keijzer *et al* 1989b) into equation (4). Figure 6(a) also shows that there is significant penetration of the light with a detectable photoacoustic contribution existing more than 0.4 μs after the onset of the rising edge of the initial compressional part of the thermoelastic wave. This corresponds to a depth of 0.63 mm. Values of μ_{eff} were found to be consistent for the majority of the nine specimens tested although two showed increased attenuation with μ_{eff} approaching 196 cm^{-1}. The results in figure 6(a) show good repeatability in terms of the shape and amplitude of the waves between different points on the same aorta specimen. Between different specimens, however, the shape of the initial part of the waves was found to be variable with the existence of a second peak in some cases. This is most likely due to the generation of a second thermoelastic wave at the intima–media boundary. The reason why this second peak did not appear in every aorta specimen tested is that it is likely that in some cases the thickness of the intima was very small. This results in the superposition of the two thermoelastic waves so that they appear as a single wave. It is also possible that the tissue was compressed when raising the jack to the extent that that the two waves were superposed. This may also account in part for variations in the measured effective attenuation coefficient and is a limitation of the experimental technique.

Measurements on three points on a single large atheromatous lesion are shown in figure 6(b). The waveforms are more complex than for normal tissue with the presence of a second peak. The first peak is due to the thermoelastic wave generated in the intima and is therefore of a similar amplitude to that produced in the normal tissue. The second peak is generated in the upper surface of the plaque mass. The shifts in the positions of the secondary peaks are due to variations in thickness of the intimal layer over the area of the lesion. Since there are no large discontinuities in the exponentially decaying rarefaction part of the wave, it is assumed that the light penetration does not extend beyond the thickness of the plaque mass into the media. Therefore, this part of the thermoelastic wave corresponds to the photoacoustic contribution from the plaque mass and, using an exponential fit, a value of $\mu_{eff} = 239$ cm^{-1} is obtained for atheroma. For other atheromatous samples

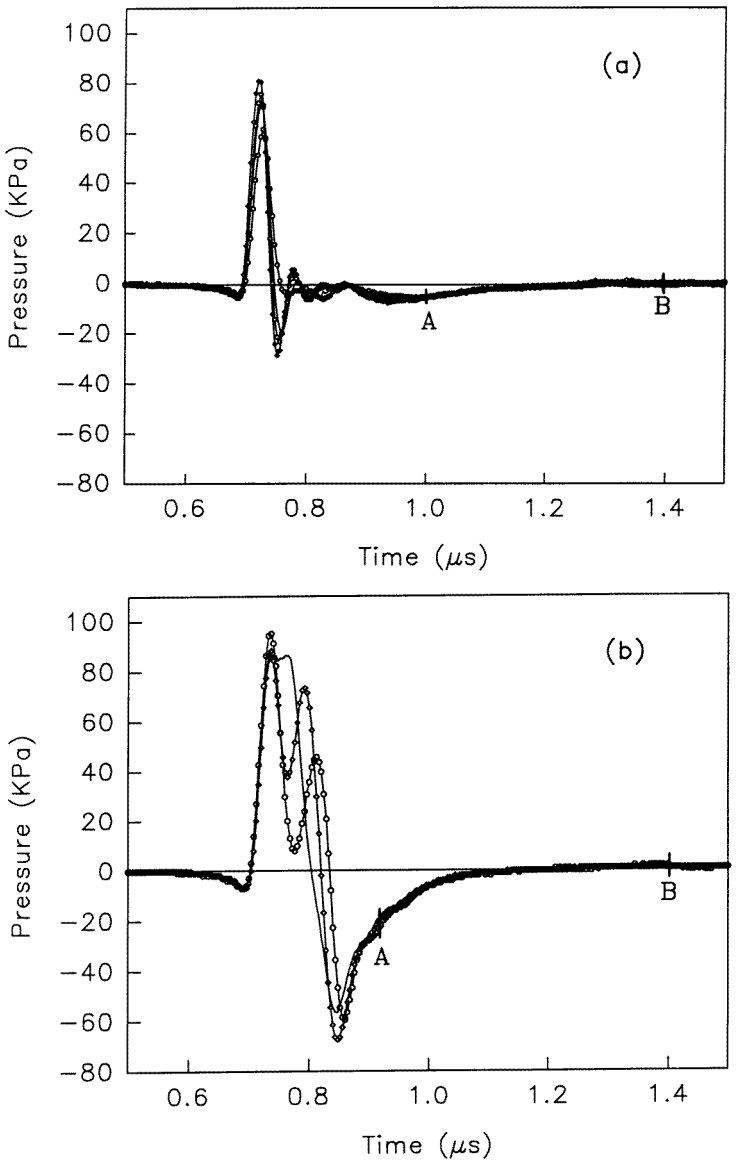

Figure 6. Thermoelastic waves generated in *post mortem* human aorta at 436 nm: (a) normal aorta (four positions) and (b) atheromatous aorta (three positions). μ_{eff} is calculated by fitting an exponential between A and B. Incident fluence, 0.17 mJ mm^{-2}, pulse duration, 13 ns; acoustic path length, 6 cm.

there was wide variation in the shape of the wave and the values of μ_{eff} calculated. This is due to variations in lesion thickness, composition and complexity. It was noted that μ_{eff} fell to approximately 112 cm^{-1} (close to the value of normal tissue) in several cases. This is because the plaque mass was relatively thin and the decaying rarefaction part of the wave to which the exponential was fitted was associated with the photoacoustic contribution

from the media rather than the atheroma. To overcome this problem and obtain a clearly interpretable waveform for thin plaque layers, higher temporal resolution is required. This could be achieved by using shorter optical pulses to generate the thermoelastic waves and increasing the bandwith of the detector.

The waveforms in figure 6 show that there is a clear difference in the characteristics of the thermoelastic waves generated in normal and atheromatous tissue. The preferential absorption in atheroma is demonstrated by the increased amplitude and effective attenuation coefficient. There was however considerable variation in the photoacoustic signatures between different specimens and discrimination between the two tissue types was not always obvious.

$\lambda = 461$ *nm*. At this wavelength, the efficiency of the Raman cell is very low. Consequently, the amplitudes of the thermoelastic waves are very close to the detection limit of the experimental arrangement. To obtain μ_{eff}, the individual waveforms shown in figures 7(a) and (b) were averaged and an exponential fitted to the averaged waveforms between points A and B.

Typical waveforms generated in normal tissue are shown in figure 7(a). Peak pressures using an incident fluence of 0.013 mJ mm^{-2} are of the order of 2 KPa. A value of $\mu_{eff} = 97$ cm^{-1} was obtained, which is considerably higher than the value of $\mu_{eff} = 35.4$ calculated from the data in table 1. Repeatability was found to be excellent both for different positions on the same specimen and between the five specimens studied.

The waveforms generated in atheroma are shown in figure 7(b). The amplitudes of the thermoelastic waves generated are about twice those of the corresponding waveforms for the normal tissue. A value of $\mu_{eff} = 187$ cm^{-1} was obtained, demonstrating the strong preferential optical attenuation at this wavelength. The characteristics of the photoacoustic signatures were found to be highly reproducible between different specimens. In each case the waveforms produced in atheroma were a simple bipolar shape, indicating that the thermoelastic contribution arises essentially from the plaque mass without the presence of secondary waves generated at boundaries. At this wavelength, it is concluded that a clearly identifiable and reproducible photoacoustic signature indicating the presence of atheromatous plaque can be obtained.

$\lambda = 532$ *nm*. The waveforms shown in figure 8 were obtained using 532 nm and the same aorta specimens as used to obtain the results at 436 nm shown in figure 6. In normal tissue (figure 8(a)), the shape of the thermoelastic waves are similar to those shown in figure 6(a) at 436 nm. The amplitude at 532 nm, however, is much smaller and the optical penetration greater due to lower absorption. This is demonstrated by the appearance of a second thermoelastic wave (S) occurring at about 0.74 μs after the initial signal. This is due to the light penetrating the full thickness of the tissue and generating a thermoelastic wave in the steel block beneath the sample. μ_{eff} was calculated to be approximately 92 cm^{-1} compared to $\mu_{eff} = 26$ cm^{-1} obtained using the data in table 1.

In atheromatous areas, the peak pressure amplitudes were similar to those of the normal tissue. The shape of the waves, however, is quite different with a triple-peak structure due to the generation of subsurface waves in the upper and lower boundaries of the plaque mass. A thermoelastic wave is not generated in the steel block beneath the sample, indicating that the light does not penetrate the full thickness of the tissue. There are two reasons for this. Firstly, the atheromatous tissue is thicker than the normal tissue and, secondly, the increased amplitudes and reduced decay times of thermoelastic waves suggest significantly higher attenuation. In these particular measurements on atheromatous tissue, μ_{eff} was calculated at 168 cm^{-1}. This is in contrast to the data of Prince *et al* (1986), which suggest that the difference in the optical properties of normal and atheromatous tissue at 532 nm is

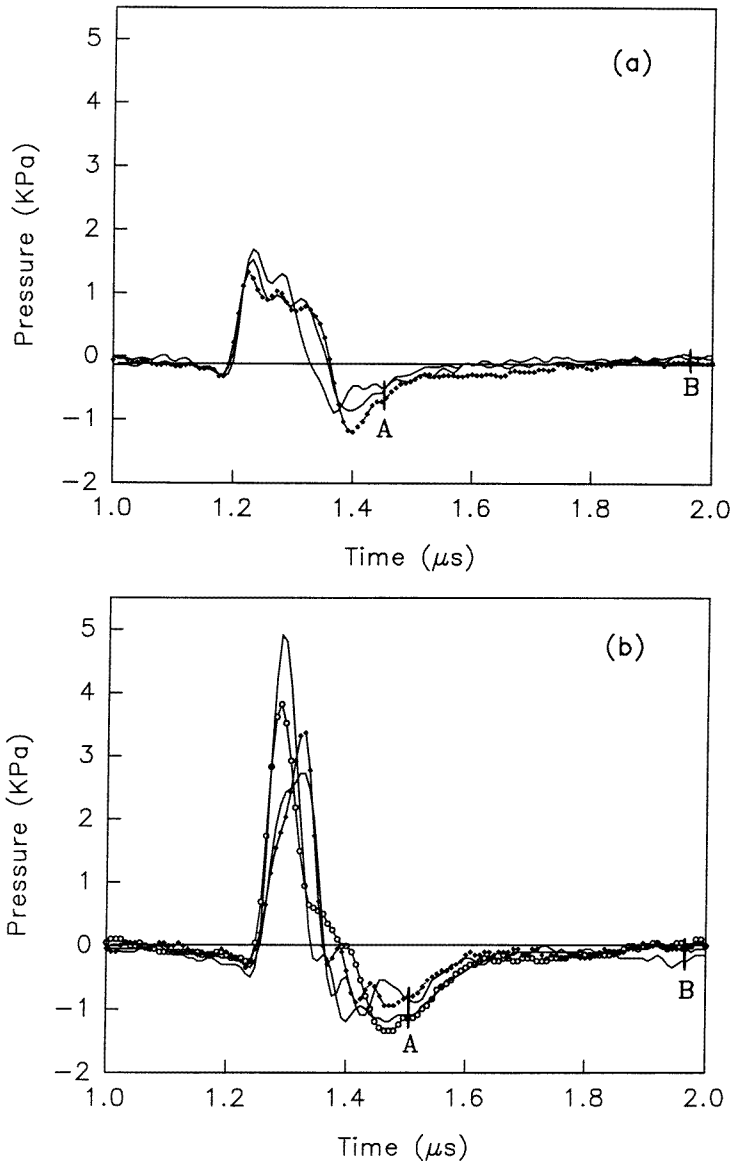

Figure 7. Thermoelastic waves generated in *post mortem* human aorta at 461 nm. (a) normal aorta (three positions) and (b) atheromatous aorta (four positions). μ_{eff} is calculated by fitting an exponential between A and B. Incident fluence, 0.013 mJ mm^{-2}; pulse duration, 13 ns; acoustic path length, 6 cm.

small. When considering all of the measurements made at 532 nm, a significant number did not show this increased absorption. In almost all cases, light penetrated the full thickness of a sample of normal tissue. In some cases, light penetrated atheromatous tissue, although this was strongly dependent upon the thickness of the lesion.

The penetration of 532 nm light through the tissue suggests that spatial information

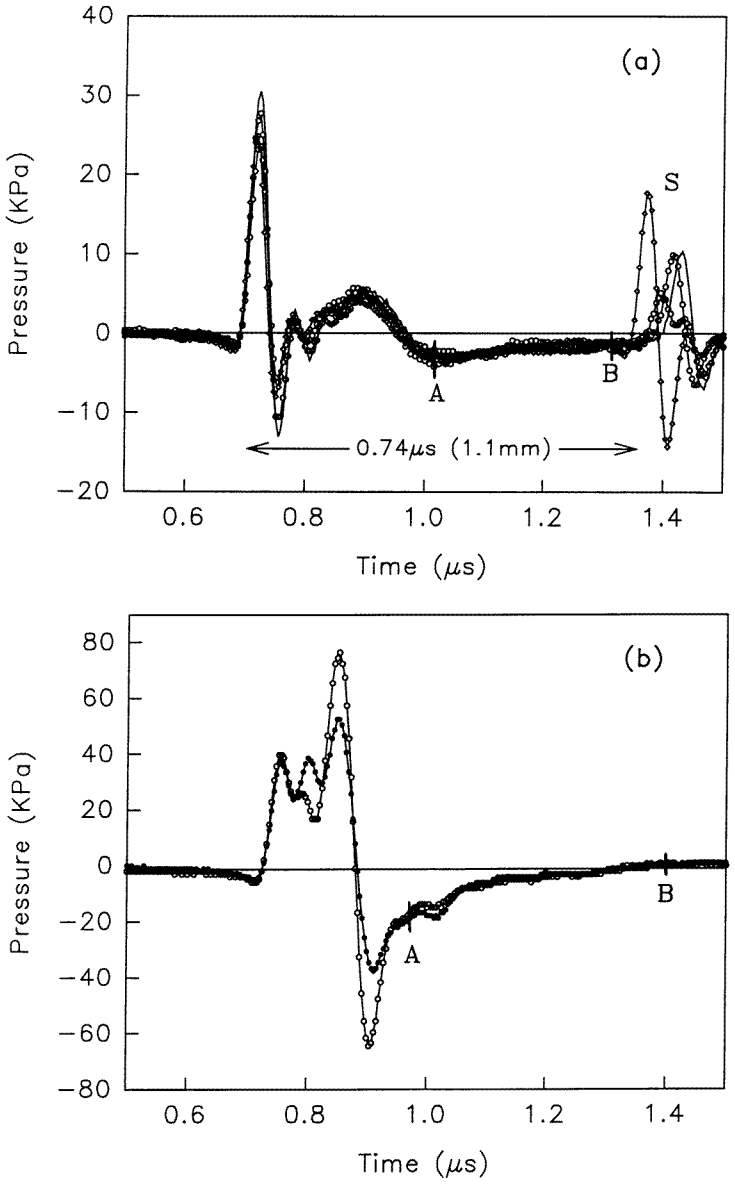

Figure 8. Thermoelastic waves generated in *post mortem* human aorta at 532 nm: (a) normal aorta (four positions)—S is the thermoelastic wave generated by light penetrating through the full thickness of tissue to the steel block beneath the tissue sample; (b) Atheromatous aorta (two positions). μ_{eff} is calculated by fitting an exponential between A and B. Incident fluence, 0.17 mJ mm^{-2}, pulse duration, 15 ns; acoustic path length, 6 cm.

describing the structure and thickness of the tissue can be obtained. To investigate this in more detail, the experiment was repeated using a sample in which the fat layer was not removed. A Perspex block was placed underneath the sample in place of the steel block and the jack raised until the surface of the tissue made light contact with the Perspex window.

Care was taken to ensure that the tissue was compressed as little as possible so that the fat layer was at least 1 cm thick. This ensured that the arrivals of any acoustic reflections from the surface of the Perspex block were sufficiently delayed that they did not coincide with any part of the initial thermoelastic wave. The results are shown in figure 9. A small signal (X) is generated at the adventitia–fat boundary, appearing around 1 μs after the initial signal (thick line). This corresponds to a depth of 1.4 mm, which is about the thickness of human aorta. To confirm this (and ensure that this signal is not an acoustic reflection artefact arising from the experimental set-up) the tissue was compressed a little by raising the jack slightly. The signal generated in the adventitia moved to the left (Y) as did the latter part of the initial thermoelastic wave (thin line). R is a reflection within the Perspex window and so its position remains constant. Thus, by using a wavelength that penetrates deep into the tissue, it is possible to obtain spatial information.

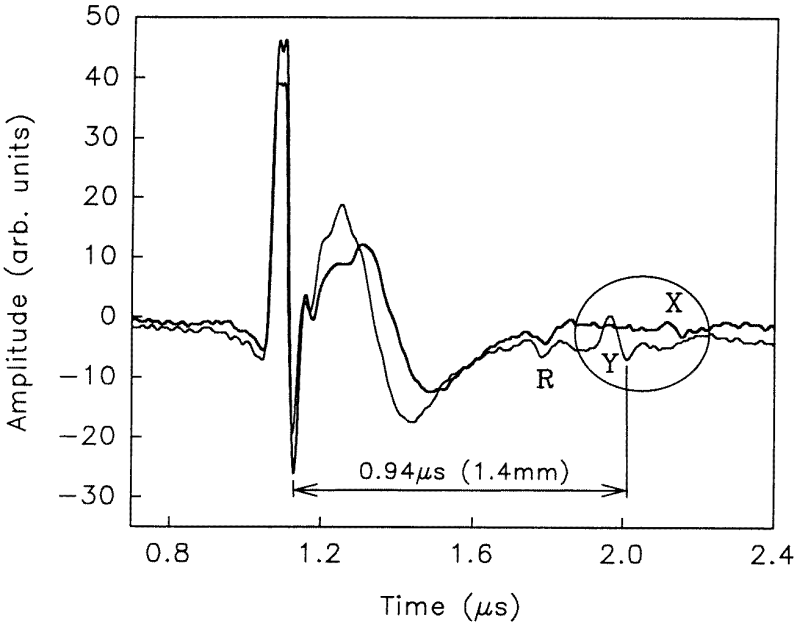

Figure 9. Thickness measurement of normal *post mortem* human aorta by generation of subsurface thermoelastic waves. A wave generated in adventitia at X (thick line) moves to Y (thin line) when the tissue sample is compressed. R reflection within the Perspex window of the experimental arrangement.

5. Discussion and conclusions

From these experiments, it is concluded that time resolved photoacoustic spectroscopy can be used to characterize arterial tissue for the purpose of discriminating between normal and atheromatous tissue. By suitable choice of wavelength, information about the composition, structure and thickness of arterial tissues can be obtained. At 436 nm, the wide variation in the photoacoustic signature makes it unsuitable for exploiting preferential absorption. In addition its relatively high absorption in both tissue types makes it unsuitable for

thickness measurements by generation of subsurface thermoelastic waves. At 461 nm, the photoacoustic signature of soft yellow lipid plaques was significantly different to that of normal tissue as a result of the strong preferential absorption in atheroma at this wavelength. This effect was found to be highly reproducible, making photoacoustic generation at 461 nm a reliable indicator of the presence of this type of plaque. At 532 nm, the lower absorption enabled the light to penetrate the full thickness of the tissue producing a photoacoustic contribution from each point in the tissue. This provided information about the structure and enabled the thickness of the tissue to be determined. Subsurface reflections arising from acoustic impedance mismatches at boundaries within the tissue were not observed in any of the experiments at any wavelength in this study. Significantly higher detection sensitivities are required for this.

Although the experimental technique was calibrated with a liquid absorber of known optical properties, the absolute values of the effective attenuation coefficients obtained in tissue were found to be significantly higher than the values calculated from the data of Keijzer *et al* (1989b). Since reported measurements of optical coefficients in soft tissue differ widely, it is difficult to say whether this apparent disagreement is due to the experimental technique and analysis used or simply due to the different morphology of the samples used in this particular study. The apparent lack of reproducibility in the photoacoustic signatures of different specimens can also be attributed to the wide variations in tissue morphology, particularly when studying atheroma. It could therefore be considered that the variation in photoacoustic signatures is an expression of the range and diversity of atherosclerotic lesions and demonstrates the applicability of the technique to characterizing complex multilayered tissues.

It is of particular interest to use a wavelength such as 532 nm which penetrates the tissue but is sufficiently strongly absorbed to generate detectable subsurface thermoelastic waves. Since the photoacoustic signature at this wavelength provides spatial information about the structure of an atheromatous lesion as well as the total thickness of the tissue, it is possible that characterization might be carried out in this way as an alternative to exploiting the preferential absorption characteristics in atheroma. Furthermore, since a significant number of atherosclerotic lesions may contain few or no carotenoids, characterization by analysis of thickness information obtained using 532 nm may prove to be more useful when studying a wide range of lesion types. It is also considerably easier to obtain 532 nm using a frequency doubled, Q switched, Nd:YAG laser than to obtain a laser wavelengths of around 470 nm.

Only soft yellow plaques have been considered in this study. The full range of fibrous–fatty and calcified lesions requires investigation. In addition, higher temporal resolution would be useful to avoid the superposition problem in which some of the temporal charactersitics relating to the plaque mass are lost. Whether pulsed photoacoustic spectroscopy will find *in vivo* application or remains an *in vitro* laboratory characterization tool will depend largely upon the success of systems currently under evaluation for the intraluminal implementation of the technique.

Acknowledgments

The authors wish to thank G Paltauf for helpful discussions on acoustic diffraction effects. A J MacRobert is acknowledged for suggesting the use of a Raman shifter for this work. E Draguioti is acknowledged for measuring the optical properties of the ink absorber. This work was supported by the British Heart Foundation.

References

Al Dhahir R K, Dyer P E and Zhu Z 1990 Photoacoustic studies and selective ablation of vascular tissue using a pulsed dye laser *Appl. Phys.* B **51** 81–5

Andersson-Engels S, Johansson J, Stenram U, Svanberg K and Svanberg S 1990 Malignant tumor and atherosclerotic plaque diagnosis using laser induced fluorescence *IEEE J. Quantum Electron.* **26** 2207–16

Baraga J J, Feld M S and Rava R P 1992 *In situ* optical histochemistry of human artery using near infrared Fourier transform Raman spectroscopy *Proc. Natl Acad. Sci. USA* **89** 3472–7

Beard P C and Mills T N 1995 Evaluation of an optical fibre probe for *in vivo* measurement of the photoacoustic response of tissues *Proc. SPIE* vol 2388, pp 446–57

——1996 Extrinsic optical fibre ultrasound sensor using a thin polymer film as a low finesse Fabry–Perot interferometer *Appl. Opt.* **35** 663–75

Boulnois J 1986 Photophysical processes in recent medical laser developments: a review *Lasers Med. Sci.* **1** 47–66

Bozhkov A I, Bunkin F V, Kolomenskii A A and Mikhalevich V G 1981 Thermo-optical methods of sound excitation in a liquid *Sov. Sci. Rev.* A **3** 459–553

Carome E F, Clark N A and Moeller C E 1964 Generation of acoustic signals in liquids by ruby laser-induced thermal stress transients *Appl. Phys. Lett.* **4** 95–7

Chen Q X, Davies A, Dewhurst R J and Payne P A 1993 Photo-acoustic probe for intra-arterial imaging and therapy *Electron. Lett.* **29** 1632–33

Chong W K, Lawrence R, Gardner J and Lees W R 1993 The appearance of normal and abnormal arterial morphology on intravascular ultrasound *Clin. Radiol.* **48** 301–6

Clarke R H, Hanion E B, Isner J M and Brody H, 1987 Laser Raman spectroscopy of calcified atherosclerotic lesions in cardiovascular tissue *Appl. Opt.* **26** 3175–7

Clarke R H, Wang Q and Isner J M 1988 Laser Raman spectroscopy of atherosclerotic lesions in human coronary artery segments *Appl. Opt.* **27** 4799–800

Crazzolara H, Von Muench W, Rose C, Thiemann U, Haase K K, Ritter M and Karsch H, R 1991 Analysis of the acoustic response of vascular tissue irradiated by an ultraviolet laser pulse *J. Appl. Phys.* **70** 1847–9

Cross F W, Al-Dhahir R K, Dyer P E and MacRobert A J 1987 Time-resolved photoacoustic studies of vascular tissue ablation at three laser wavelengths *Appl. Phys. Lett.* **50** 1019–21

Deckelbaum I L, Lam J K, Cabin H S, Soni Clubb K and Long M B 1987 Discrimination of normal and atherosclerotic aorta by laser induced fluorescence *Lasers Surg. Med.* **7** 330–5

Goss S A, Johnston R L and Dunn F 1978 Comprehensive compilation of empirical ultrasonic properties of mammalian tissues *J. Acoust. Soc. Am.* **64** 423–57

Gournay L S 1966 Conversion of electromagnetic to acoustic energy by surface heating *J. Acoust. Soc. Am.* **40** 1322–30

Greenleaf J F, Duck F A, Samayoa W F and Johnson S A 1974 Ultrasonic data acquisition and processing system for atherosclerotic tissue characterization *Ultrasonic Symp. Proc. IEEE* 74CH0896-ISU pp 738–43

Gussenhoven E J *et al* 1989 Arterial wall characteristics determined by intravascular ultrasound imaging: an *in vitro* study *J. Am. Coll. Cardiol.* **14** 947–52

Keijzer M, Jacques S L, Prahl S A and Welch A J 1989a Light distributions in artery tissue: Monte Carlo simulations for finite-diameter laser beams *Lasers Surg. Med.* **9** 148–54

Keijzer M, Richards-Kortum R R, Jacques S L and Feld M S 1989b Fluorescence spectroscopy of turbid media: autofluorescence of the human aorta *Appl. Opt.* **28** 4286–92

Long F H and Deutsch T F 1987 Pulsed photothermal radiometry of human artery *IEEE J. Quantum Electron.* **23** 1821–5

Mason W P and Thurston R N (ed) 1988 *Physical Acoustics* vol 18 (San Diego, CA: Academic) ch 2, pp 30–1

Mills TN 1988 Photoacoustic ultrasound for guidance at laser angioplasty (abstract) *Mini-Symp. on Sensors for Medical Laser Applications* (Broadway: Rank Prize Funds)

Mills T N, Andrews S M L and Essenpreis M 1991 Pulsed laser generation and optical fibre detection of thermoelastic waves in arterial tissues (abstract) *Lasers Surg. Med.* (suppl 3) 4

Oraevsky A A, Jacques S L, Pettit G H, Sauerbrey R A, Tittel F K, Nguy J H and Henry P D 1993 XeCl laser-induced fluorescence of atherosclerotic arteries: spectral similarities between lipid-rich lesions and peroxidised lipoproteins *Circulation Res.* **72** 84–90

Oraevsky A A, Letokhov V S, Ragimov S E, Omel Yanenko V G, Belyaev A A, Shekhonin B V and Akchurin R S 1988 Spectral properties of human atherosclerotic blood vessel walls *Lasers Life Sci.* **2** 275–88

Paltauf G, Frenz M and Schmidt-Kloiber H 1996 Laser induced micro bubble formation at a fiber tip in absorbing media: experiments and theory *Proc. SPIE* vol 2624 (Bellingham, WA: SPIE) pp 72–82

Patel C K N and Tam A C 1981 Pulsed optoacoustic spectroscopy of condensed matter *Rev. Mod. Phys.* **53** 517–50

Prince M R, Deutsch T F, Matthews-Roth M M, Margolis R, Parrish J A and Oseroff A R, 1986 Preferential light absorption in atheromas in vitro–implications for laser angioplasty *J. Clin. Invest.* **78** 295–302

Rooney J A, Gammell P M, Hestenes J D, Chin H P and Blankenhorn D H 1982 Velocity and attenuation of sound in arterial tissues *J. Acoust. Soc. Am.* **71** 462–66

Sigrist M W 1986 Laser generation of acoustic waves in liquids and gases *J. Appl. Phys.* **60** 83–121

Star W M, Marijnissen J P A and van Gemert M J C 1988 Light dosimetry in optical phantoms and in tissues: 1. Multiple flux and transport theory *Phys. Med. Biol.* **33** 437–54

Terzic M and Sigrist M W 1984 Diffraction characteristics of laser-induced acoustic waves in liquids *J. Appl. Phys.* **56** 93–5

Van Gemert M J C, Verdaasdonk R, Stassen E G, Schets G A C M, Gijsbers G H M and Bonnier J J 1985 Optical properties of human blood vessel wall and plaque *Lasers Surg. Med.* **5** 235–7

Wang L and Jacques S L 1992 *Monte Carlo Modelling of Light Transport in Multi-layered Tissues in Standard C* (Houston, TX: University of Texas M D Anderson Cancer Center) ch 6, p 64